Monthly Notices
of the
ROYAL ASTRONOMICAL SOCIETY

MNRAS **450,** 2354–2366 (2015) doi:10.1093/mnras/stv806

The parent populations of six groups identified from chemical tagging in the solar neighbourhood

Alice C. Quillen,[1⋆] Borja Anguiano,[2,3] Gayandhi De Silva,[4,5] Ken Freeman,[6] Dan B. Zucker,[2,3,4] Ivan Minchev[7] and Joss Bland-Hawthorn[5]

[1]*Department of Physics and Astronomy, University of Rochester, Rochester, NY 14627, USA*
[2]*Macquarie University Research Centre in Astronomy, Astrophysics & Astrophotonics, NSW 2109, Australia*
[3]*Department of Physics & Astronomy, Macquarie University, NSW 2109, Australia*
[4]*Australian Astronomical Observatory, PO Box 296, NSW 1710, Australia*
[5]*Sydney Institute for Astronomy, School of Physics, University of Sydney, NSW 2006, Australia*
[6]*Research School of Astronomy & Astrophysics, Mount Stromlo Observatory, ACT 2611, Australia*
[7]*Leibniz-Institut für Astrophysik Potsdam (AIP), An der Sternwarte 16, D-14482 Potsdam, Germany*

Accepted 2015 April 8. Received 2015 April 7; in original form 2015 March 10

ABSTRACT

We estimate the size and distribution of the parent populations for the six largest (at least 20 stars in the solar neighbourhood) chemical groups identified in the chemical tagging experiment by Mitschang et al. Stars in the abundance groups tend to lie near a boundary in angular momentum versus eccentricity space where the probability is highest for a star to be found in the solar neighbourhood and where orbits have apocentre approximately equal to the Sun's galactocentric radius. Assuming that the parent populations are uniformly distributed at all azimuthal angles in the Galaxy, we estimate that the parent populations of these abundance groups contain at least 200 000 members. The spread in angular momentum of the groups implies that the assumption of a uniform azimuthal distribution only fails for the two youngest groups and only for the highest angular momentum stars in them. The parent populations of three thin disc groups have narrow angular momentum distributions, but tails in the eccentricity and angular momentum distributions suggest that only a small fraction of stars have migrated and increased in eccentricity. In contrast, the parent populations of the thick disc groups exhibit both wide angular momentum and eccentricity distributions implying that both heating and radial migration has taken place.

Key words: Galaxy: abundances – Galaxy: evolution – Galaxy: kinematics and dynamics – open clusters and associations: general.

1 INTRODUCTION

Freeman & Bland-Hawthorn (2002) proposed that stars with similar abundance measurements could represent a particular star formation or enrichment event, discrete in space and time, as might be expected from the homogeneity of nearby open clusters and moving groups (Quillen 2002; De Silva et al. 2006, 2007). These stars would subsequently disperse in the Galaxy, retaining their initial chemical patterns (Bland-Hawthorn, Krumholz & Freeman 2010). A search for stars that have a similar abundance pattern as the Sun would allow us to learn about the birth place of the Sun (Portegies Zwart 2009; Liu et al. 2015). Because stars in the solar neighbourhood span a wide distribution in stellar ages, metallicities and inferred birth Galactocentric radii, it is difficult to pin down the role of specific mechanisms for stellar migration and heating (increase in radial and vertical epicyclic motions; e.g. see Freeman & Bland-Hawthorn 2002; Quillen et al. 2009; Schönrich & Binney 2009; Kruijssen et al. 2011; Haywood et al. 2013; Lehnert et al. 2014; Minchev et al. 2014). A study of homogeneous groups of stars should give complementary constraints on migration and heating processes, compared to those arising from studies of heterogeneous distributions (such as a magnitude-limited sample of stars in the solar neighbourhood).

We focus on the a high-resolution spectroscopic study of 714 F and G dwarf and subgiant stars in the solar neighbourhood studied by Bensby, Feltzing & Oey (2014). The blind chemical tagging experiment by Mitschang et al. (2014) used this sample to identify groupings of nearby disc field stars that share metal abundance measurements. The field stars they identified as having

⋆ E-mail: alice.quillen@rochester.edu

Table 1. Properties of the abundance groups.

GIC	N	Age (Gyr)	[Fe/H]	[α/Fe]	$\langle L\rangle$ (km s^{-1} kpc)	σ_L	$\langle e\rangle$
5	21	4.0 ± 0.6	0.23 ± 0.04	0.01 ± 0.02	1715	214	0.14
1	42	4.8 ± 0.4	0.07 ± 0.07	0.01 ± 0.01	1748	262	0.17
3	25	7.1 ± 0.4	-0.07 ± 0.06	0.03 ± 0.02	1522	247	0.28
4	24	10.1 ± 1.4	-0.43 ± 0.05	0.18 ± 0.02	1450	271	0.32
2	30	10.2 ± 0.8	-0.30 ± 0.05	0.22 ± 0.02	1368	373	0.34
6	21	12.1 ± 1.1	-0.64 ± 0.07	0.26 ± 0.02	1297	510	0.39

Notes. GIC is the group number given by Mitschang et al. (2014). N is the number of stars in the abundance group and the estimated age by Mitschang et al. (2014) is given in Gyr. Mean [Fe/H] and [α/Fe] values in solar units for the stars in the group were computed using abundance values listed in table C.3 by Bensby et al. (2014), finding them using *Hipparcos* catalogue numbers for the stars listed in table 2 by Mitschang et al. (2014) for each group. Errors in the abundances are the standard deviations of the abundance values from each star. We list the mean $\langle L\rangle$ and standard deviation, σ_L, (in km s^{-1} kpc) of the angular momentum distributions and the mean eccentricity $\langle e\rangle$ for each group (distributions are shown in Fig. 3). These are computed from the eccentricity and angular momentum values computed by Bensby et al. (2014).

similar abundances are not clustered in space, nor do they share similar space motions. Using isochrone sets, Mitschang et al. (2014) estimated the ages of each of these chemical groupings. These groups represent a first attempt to identify groups of stars from single discrete birth events.

We ask here: What is the number and distribution in the Galaxy of a parent stellar population of one of these abundance groups? We necessarily focus on only the six largest groups identified by Mitschang et al. (2014) each of which contains more than 20 stars. We begin by assuming that the parent population for each group is currently evenly distributed (azimuthally) in the Galaxy and at the current time only a fraction of the stars in the parent population are present in the solar neighbourhood. This assumption was adopted for the toroid models by Bland-Hawthorn et al. (2010, for an illustration see their fig. 4). This assumption neglects how a cluster dissolves and is dispersed in the Galaxy (see discussions by Portegies Zwart 2009; Bland-Hawthorn et al. 2010). We will discuss how our assumption of axisymmetry for the parent distribution could have impacted our inferred parent population distributions. We also neglect our location in the Galaxy with respect to spiral and bar perturbations, (e.g. Quillen et al. 2011; Minchev, Chiappini & Martig 2013; Minchev et al. 2014; Quillen 2014). We assume that there is no correlation between vertical oscillation amplitude and eccentricity in the parent population and that the epicyclic angle distribution is relaxed (see Minchev et al. 2009 for an illustration of what can be seen when this is not true).

We first consider the fraction of time that a star with a given eccentricity and angular momentum might be seen in the solar neighbourhood.[1] From a distribution of orbits with a given eccentricity and angular momentum, we estimate the probability that a star is seen in a solar neighbourhood volume with boundary dependent on the distances of stars in the Bensby et al. (2014) sample. For each star in one of Mitschang et al. (2014) chemical groupings, the inverse of this probability lets us estimate the number of stars at similar eccentricities and angular momentum in the parent population.

Bensby et al. (2014) selected stars for spectroscopic study with a range of properties and necessarily did not observe every F and G star in the solar neighbourhood. We compare the Bensby et al. (2014) sample with the Geneva–Copenhagen survey (GCS) of F and G stars in the solar neighbourhood (Nordström et al. 2004; Holmberg, Nordström & Anderson 2009) to estimate a selection bias as a function of angular momentum. The GCS is a magnitude-limited, kinematically unbiased sample of almost 17 000 nearby F and G stars. Bensby et al. (2014) warn that their sample is a compilation of a number of different observing programs, and so they give no selection description for the entire sample. We should be careful in interpreting inferred parent distributions, keeping in mind that there might be additional biases arising from the selection of this sample.

Using these two corrections, the first based on probability for such an orbit to be seen in the solar neighbourhood, the second based on selection bias, we derive estimates for the source or parent populations of the six abundance groups identified by Mitschang et al. (2014). A discussion follows on the nature of the parent populations and on how our underlying assumptions have impacted our estimate of their number and distributions.

2 PROPERTIES OF THE SIX ABUNDANCE GROUPS

Properties of the six largest abundance groups found by Mitschang et al. (2014) are listed in Table 1. The *Hipparcos* catalogue numbers of the stars in each group are listed in table 2 by Mitschang et al. (2014). Our Table 1 lists the group identification number (from their table 2), group age (that derived by Mitschang et al. 2014 using Yonsei–Yale isochrone sets and with error estimate described in their section 4.2) the mean [Fe/H] of the group (in solar units and using abundances listed in table C2 by Bensby et al. 2014) and the group mean [α/Fe] in solar units. The mean abundance values and standard deviation for each group are computed from the values for each star in the group. For each star, [α/Fe] is calculated by averaging the abundances for α elements Ti, Mg, Si and Ca (as done by Mitschang et al. 2014). Table 1 also lists the mean $\langle L\rangle$ and standard deviation, σ_L, (in km s^{-1} kpc) of the angular momentum

[1] We only consider the z component of angular momentum that is dominated by rotation in the Galaxy. In the solar neighbourhood, the angular momentum of a star $L \approx R_{\odot}(V + V_{\mathrm{LSR},\odot})$ with $R_{\odot}$ the galactocentric radius of the Sun, V_{LSR} the rotation velocity of the LSR and V the tangential component of the star's velocity vector.

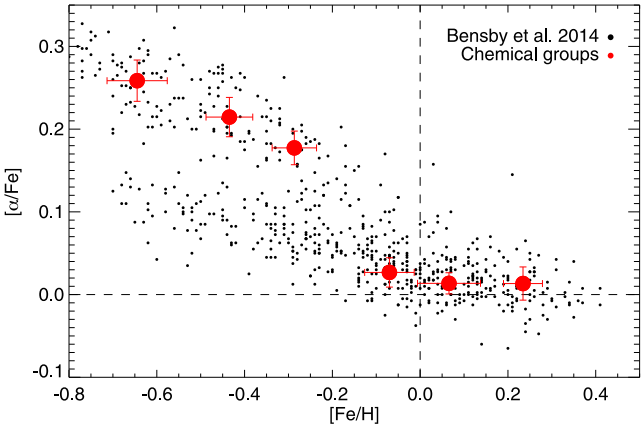

Figure 1. Mean abundances (in solar units) for each of the six abundance groups (found by Mitschang et al. 2014) are shown as large red dots. Error bars represent standard deviations of the abundance values of stars in the group. Black dots show abundances of individual stars from the Bensby et al. (2014) sample. The dashed lines show solar values. The three youngest groups are typical of the thin disc population, whereas the three oldest are typical of the thick disc population.

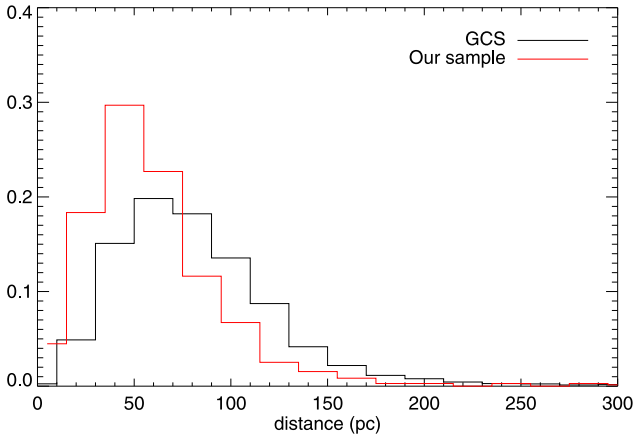

Figure 2. Distance distribution for the Bensby et al. (2014) sample compared to that of the GCS (Nordström et al. 2004; Holmberg et al. 2009). Most stars from the Bensby et al. (2014) sample are within 100 pc of the Sun. The distributions have been normalized so that they integrate to one.

distributions of each group. These are the angular momentum values by Bensby et al. (2014) who computed space motions for all the stars in their sample (see their section 3).[2]

Studies of abundance populations based on high-resolution spectroscopy find a bimodality in the abundance distribution (e.g. Fuhrmann 2011; Navarro et al. 2011; Adibekyan et al. 2013; Haywood et al. 2013; Anders et al. 2014 and references therein) with a dividing line between thin and thick discs populations near $[\alpha/\mathrm{Fe}] \sim 0.12$ (e.g. see fig. 12 by Reddy, Lambert & Allende Prieto 2006 and section 5.1 by Mitschang et al. 2014). For each abundance group, mean values of [Fe/H] are plotted against the mean values of $[\alpha/\mathrm{Fe}]$ in Fig. 1 with the other stars in the Bensby et al. (2014) sample. The three youngest groups have abundances consistent with a thin disc population, whereas the older three have abundances consistent with a thick disc population.

690 out of 714 stars in the Bensby et al. (2014) sample are also present in the GCS of F and G stars in the solar neighbourhood (Nordström et al. 2004; Holmberg et al. 2009). The distribution of distances from the Bensby et al. (2014) sample is compared to that of the GCS in Fig. 2, illustrating that the stars in the Bensby et al. (2014) sample are predominantly nearer than 100 pc. Here, distances are based on parallaxes from the new reduction of the *Hipparcos* data by van Leeuwen (2007). Of the 163 stars in the six abundance groups, we find that only nine of the stars are further than 100 pc from the Sun. Thus, this sample of stars is confined to a small spherical volume, centred on the Sun, with an approximate radius of 100 pc.

From the angular momentum, L, and eccentricity, e, values listed by Bensby et al. (2014), we constructed histograms for each group, and these are shown in Fig. 3. The mean angular momentum (also listed in Table 1) for each group decreases with increasing age, suggesting that the oldest groups arise from the inner galaxy and the youngest groups are located near the Sun's galactocentric radius.

While Bensby et al. (2014) did not list errors for eccentricity e or angular momentum L for each star, we can assume that the space velocity components U, V, W have errors the same size as those of the GCS which are estimated to be $\Delta v \sim 1.5$ km s^{-1} (see section 4.7 by Nordström et al. 2004). This corresponds to an approximate error of $\Delta L \sim 13$ km s^{-1} kpc in angular momentum. We estimate the size of an error in eccentricity with $\Delta e \sim \Delta v / V_{\mathrm{LSR},\odot} \sim 0.01$. The errors could also have systematic trends in them (as a function of other parameters such as position on the sky) and due to uncertainty in the solar motion or the rotation curve used to calculate the eccentricity.[3]

3 PROBABILITY OF DETECTING A STAR IN THE SOLAR NEIGHBOURHOOD AS A FUNCTION OF ORBITAL ECCENTRICITY AND ANGULAR MOMENTUM

In this section, we describe how to estimate the probability that a star with a given angular momentum and eccentricity is found in a solar neighbourhood sample if the parent population is randomly distributed in azimuthal and epicyclic angles. We use angular momentum and eccentricity to describe each orbit. We use eccentricity e instead of energy as it is unitless, describes the extent of radial excursion in the orbit and so gives an intuitive description for the orbit shape, and it does not depend on a potential energy offset.

To be consistent with the angular momentum and eccentricities computed by Bensby et al. (2014) and Mitschang et al. (2014), we use the same Galactic potential model as they did to compute our probabilities. Using the gravitational potential for the Galactic model by Allen & Santillan (1991)[4], we integrate planar orbits with different initial angular momentum and different initial radii.

[2] The adopted LSR $(U_\odot, V_\odot, W_\odot) = (11.10, 12.24, 7.25)$ km s^{-1} is that by Schönrich, Binney & Dehnen (2010).

[3] At low eccentricity, the difference $E - E(L) \sim 0.5\kappa^2 r_g^2 e^2$, where r_g is the guiding radius, e is the orbital eccentricity, E is the orbital energy per unit mass, $E(L)$ is the energy (per unit mass) of a circular orbit with angular momentum L and κ is the epicyclic frequency. For a power-law rotation curve $v_c(r) \propto r^{-\alpha}$, the epicyclic frequency $\kappa = \sqrt{2(1-\alpha)}\Omega$, where the angular rotation rate $\Omega = v_c/r$. Uncertainty in the slope of the rotation curve affects the estimate for $E(L)$ and epicyclic frequency, κ, and so the computed values for the eccentricity.

[4] This model assumes that a Galactocentric distance for the Sun and rotation velocity of a circular orbit at that radius of $\mathrm{R}_\odot = 8.5$ kpc and $V_{\mathrm{LSR},\odot} = 220$ km s^{-1}. With these values the angular momentum of the LSR is $L_{\mathrm{LSR}} = 1870$ km s^{-1} kpc.

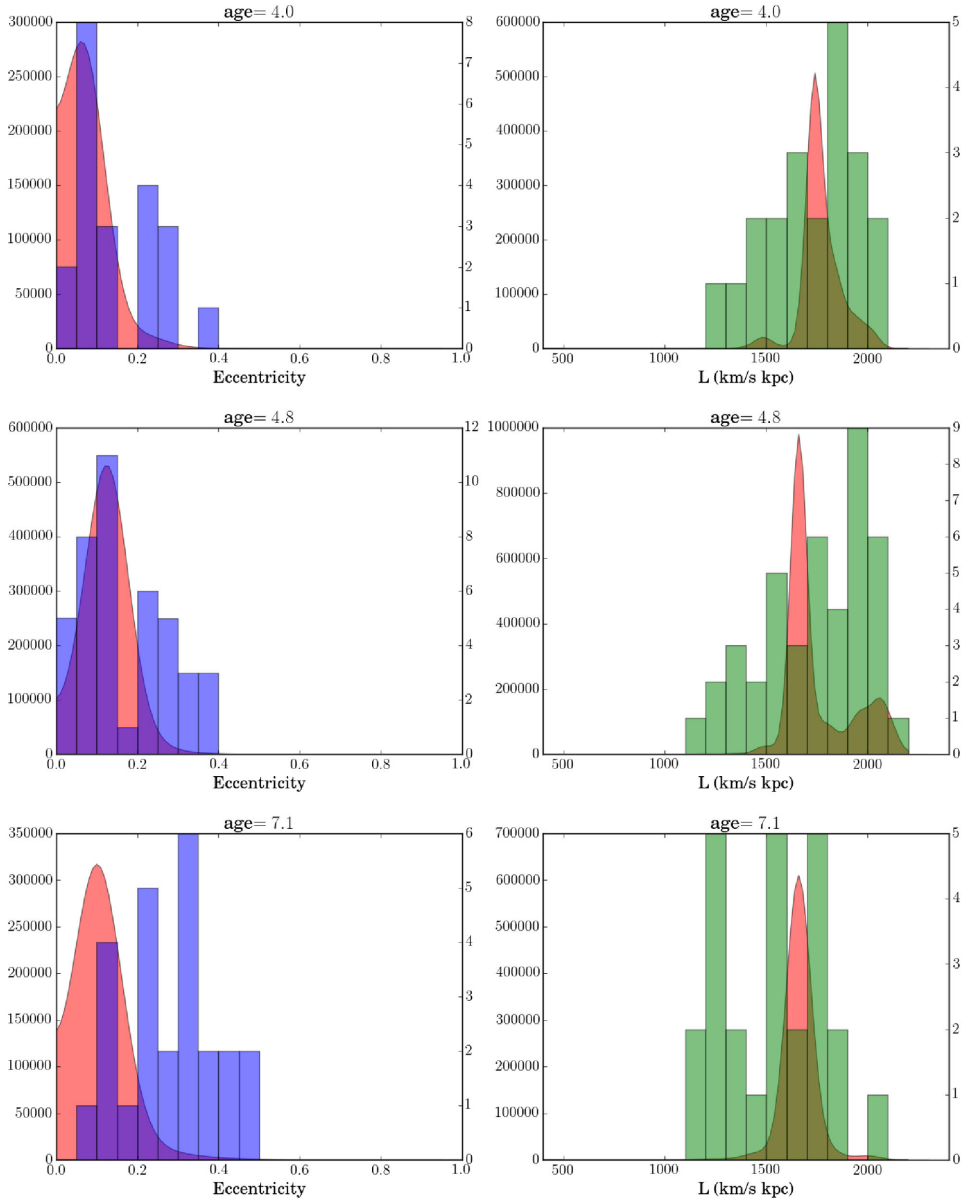

Figure 3. Eccentricity and angular momentum distributions of the six groups. The left-hand panels show the eccentricity distributions and the right-hand panels show the angular momentum distributions. Each row shows a different group, with group labelled by age. Shown in blue with axis on the right-hand side of the left-hand panels are the observed eccentricity distribution of each group, plotting numbers of stars in bins of width 0.05 in eccentricity. Shown in green, with axis on the right-hand size of the right-hand panels are the angular momentum distributions of each group, showing the number of stars in bins of width 100 km s^{-1} kpc. The pink shaded regions, corresponding to axes on the left-hand side of each panel, show the estimated numbers stars in the parent population distributions (corrected for selection and assumed to be evenly distributed in azimuthal angle, see Section 4) with bin widths of 0.01 in eccentricity or 20 km s^{-1} kpc in angular momentum.

For each orbit, we record the eccentricity defined as $e = (R_a - R_p)/(R_a + R_p)$ (following Bedin et al. 2006), where R_a, R_p are radii of galactic apocentre and pericentre, respectively.

For each e, L, we computed a few thousand positions in a full orbit (using a finite size timestep to compute a full orbital period). We then randomly chose a few thousand azimuthal angles (corresponding to randomly chosen initial orientations) giving a total of approximately 10 million points in the galaxy plane to compute each probability. At each timestep and for each angle, we computed the position of the star and the fraction that fell within a solar neighbourhood area, within 100 pc of the Sun, gave the probability. For randomly distributed initial azimuthal angle and initial position in the orbit, and using a single orbital period, we measure the fraction of stars in an orbit, as a function of angular momentum and eccentricity, that are located within 100 pc of the Sun. In other words, we assume that there is a distribution of orbits with this angular momentum and eccentricity that is randomly distributed in azimuthal angle, and using this distribution, we compute the probability, $p_o(e, L)$, that a star would be observed in the solar neighbourhood at any particular time. For a range of orbital eccentricities, e, and angular momenta, L, we compute $p_o(e, L)$ and display it in Fig. 4. The colour bar shows the $\log_{10}$ of the probability. The black dots show the orbits that we integrated and that were used to make the colour contours. The angular momentum is in units of km s^{-1} kpc.

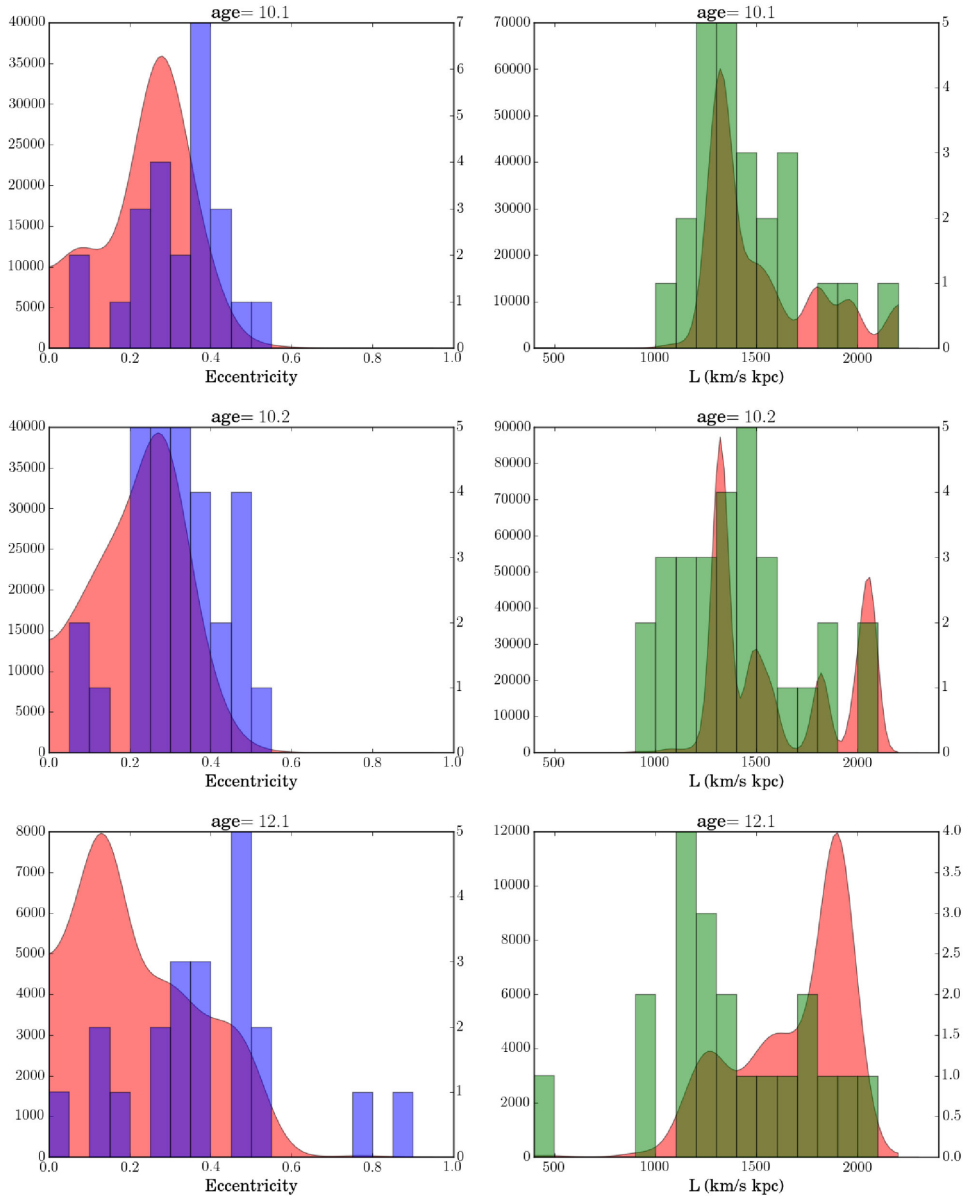

Figure 3 – *continue.*

Wiggles in Fig. 4 are artefacts due to the sampling of the orbits integrated.

At low eccentricity and angular momentum L above or below that of the local standard of rest (LSR), the probability p_o, for the orbit is zero as the orbit never crosses the Sun's galactocentric radius. A star in such an orbit is never near the Sun. The white region on the lower left and upper left in Fig. 4 is the forbidden region. Large eccentricity orbits that do cross the Sun's galactocentric radius (on the right in Fig. 4) are less probable than lower eccentricity ones as stars spend much of the time at larger or smaller galactocentric radius than that of the Sun. For a given angular momentum, the probability is highest at an eccentricity that just barely allows the orbit to cross into the solar neighbourhood. We attribute the increase in probability near the forbidden region boundary to the large fraction of the orbital period spent near a particular radius when at apocentre or pericentre. This effect has previously been described as a bias due to *crossing times* in the solar neighbourhood (Mayor, Martinet & Turon Lacarrieu 1977). The effect is illustrated in Fig. 5 showing epicyclic oscillations for three different groups of orbits, one with apocentre near the Sun's galactocentric radius that is likely to be seen in the solar neighbourhood, high-eccentricity orbits that have a lower probability and orbits within the forbidden region that cannot be found in solar neighbourhood.

We can account for this probability increase near apocentre using an epicyclic approximation for radial orbital variations. For low-eccentricity stars the radius $r(t) \approx r_g(1 + e\cos(\kappa t + \phi_0))$, where r_g is the guiding radius, e is the eccentricity, κ is the epyclic frequency, ϕ_0 an initial phase and the apocentre radius $R_a = r_g(1 + e)$. Near apocentre and using a small angle approximation, $R_a - r(t) \propto (t - t_{apo})^2$, where t_{apo} is a time when the orbit is at apocentre. This gives a dependence of the fraction of the orbital period, f, spent within a narrow annulus of width dr from apocentre, $f \propto \sqrt{dr}$. In contrast, when the orbit is near the guiding radius and using a small angle approximation, $r - r_g \propto (t - t_g)$ (with t_g a time the orbit

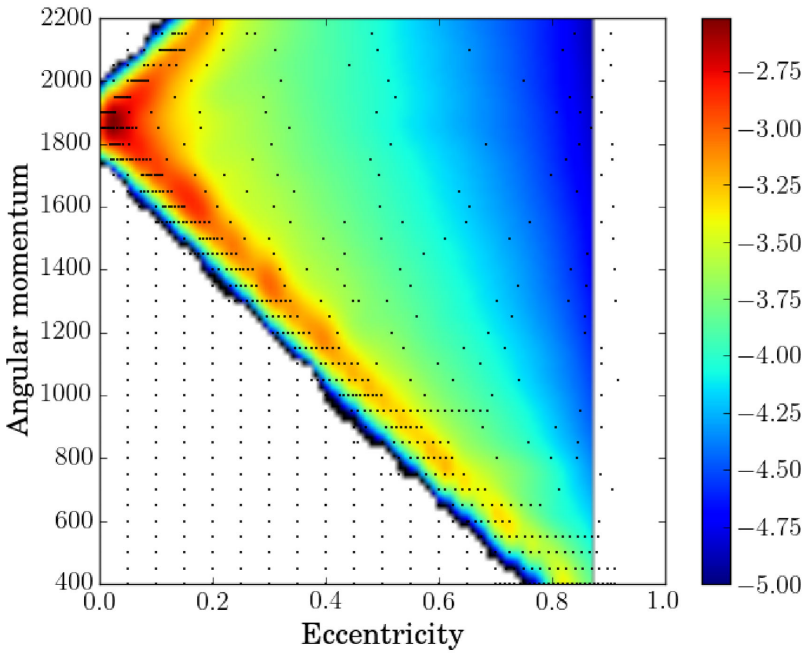

Figure 4. As a function of orbital eccentricity and angular momentum, we show $\log_{10} p_o(e, L)$ of the probability that a distribution of stars in such an orbit (but with randomly chosen angles) would be observed in the solar neighbourhood (100 pc from the Sun). The probability is computed using planar orbits integrated in the Galactic potential model by Allen & Santillan (1991). Each orbit integrated is shown as a black dot. The angular momentum is in units of km s^{-1} kpc.

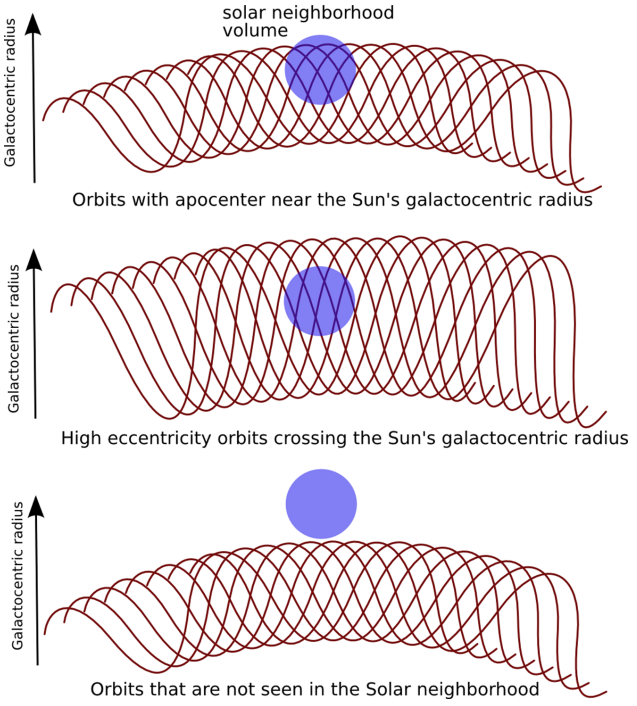

Figure 5. Orbits with apocentre near Sun's galactocentric radius (as shown on the top) are more likely to be seen in a solar neighbourhood sample, than a high-eccentricity orbit (as shown in the middle). The bottom illustrates orbits that never are found in the solar neighbourhood, corresponding to a region in e, L space that we call the forbidden region.

crosses the guiding radius) giving a dependence of the fraction of the orbital period spent within dr of r_g to be $f \propto dr$. For a small range of radius dr, the fraction of the orbital period spent near apocentre is larger than that spent near the middle of the orbit at the guiding radius. The trend is still present at moderate eccentricity where the epicyclic approximation is less accurate.

3.1 Probabilities of individual abundance group stars

We now consider the probabilities that stars in the abundance groups are seen in the solar neighbourhood. In Fig. 6, we show the eccentricity and angular momentum of stars in these abundance groups on top of the probability, p_o, that such a star is found in the solar neighbourhood. Each panel shows a different abundance group and the groups are labelled by their ages. The probability is displayed as in Fig. 4. Fig. 6 illustrates that stars tend to be found near the forbidden region in e, L space, as expected from the location of the high values in probability distribution $p_o(e, L)$.

For each star with eccentricity e_i and angular momentum L_i, we can use the probability $p_o(e_i, L_i)$ to estimate the size of the parent grouping. The parent population has at least

$$N_1 = \sum_i \frac{1}{p_o(e_i, L_i)} \quad (1)$$

stars in it. If we underestimate the probability $p_o(e_i, L_i)$, then we will overestimate the number of stars in the parent population. To ensure that observational errors in e_i and L_i for individual stars do not give spurious high numbers near the forbidden region, we take p_o to be the maximum value within $e_i \pm \Delta e$ and $L_i \pm \Delta L$ with $\Delta e = 0.01$ and $\Delta L = 13$ km s^{-1} kpc, the size of the errors estimated for these quantities (see the end of Section 2). For each abundance group, we have summed-up the inverse of the probabilities and list the total number of estimated parent stars in Table 2.

4 PARENT POPULATION DISTRIBUTIONS

Using the probabilities estimated for each star in an abundance grouping, we now estimate the number density of stars in the

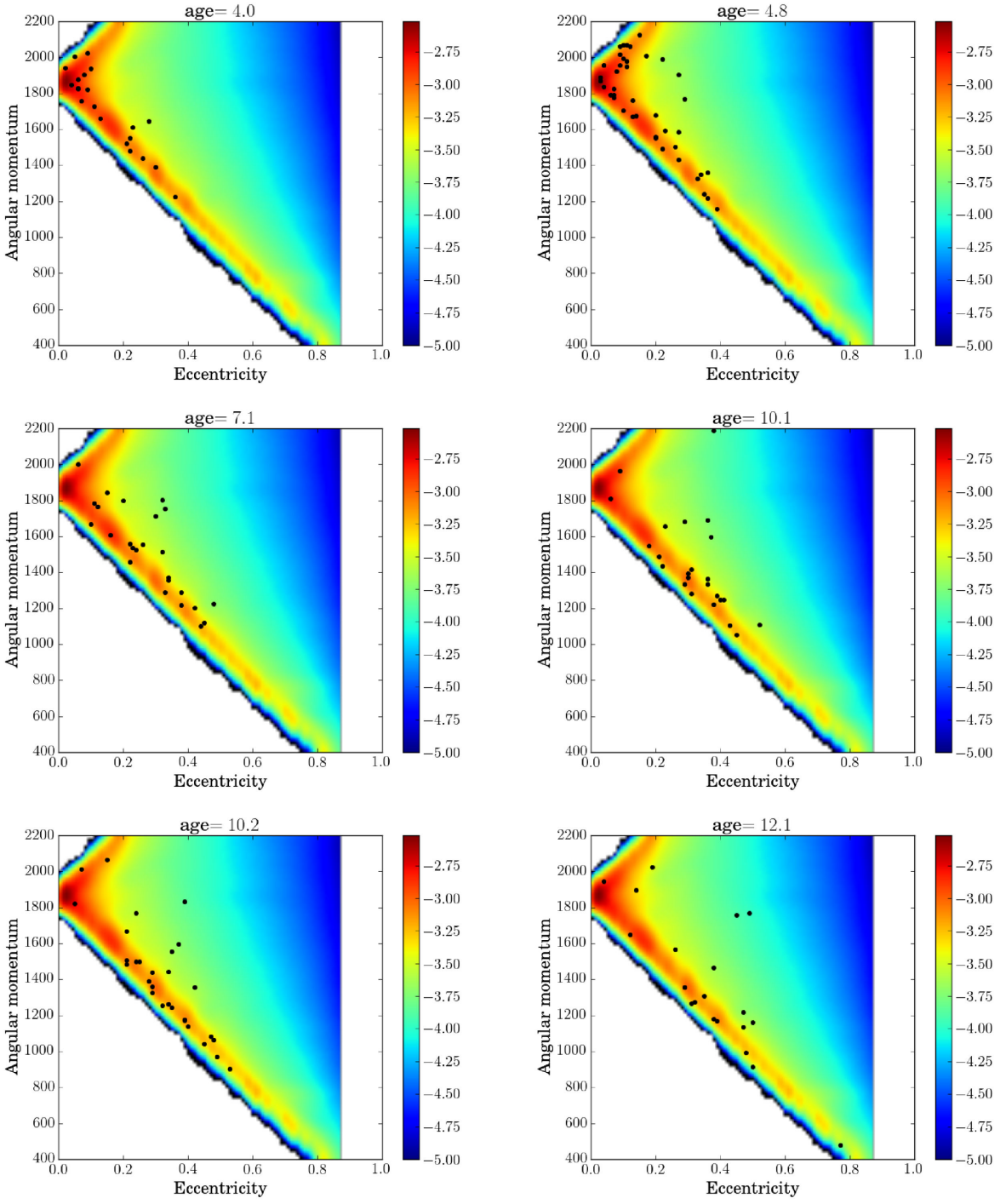

Figure 6. Eccentricity and angular momentum of stars in an abundance group plotted as points on top of the probability that such an orbit is detected in the solar neighbourhood. Each panel shows a different abundance group, and the groups are labelled by their ages. The colour bar shows $\log_{10} p_o$ of the probability computed for each orbit. The stars in each abundance group often lie in regions of high probability, near the boundary of the forbidden region.

grouping as a function of eccentricity and angular momentum e, L. Each star with e_i, L_i contributes a total parent population of $p_o(e_i, L_i)^{-1}$ at e_i, L_i. We smooth this distribution to estimate the number density of stars in the parent population as a function of e, L. For each cluster, the resulting distributions in e and L are shown in Fig. 7. The colour bars show the number of stars per eccentricity and angular momentum bin with bin size $de = 0.01$ and $dL = 20$ km s^{-1} kpc. The distributions have been smoothed by four or five eccentricity bins and two or three angular momentum bins with the tighter distributions (for the younger groups) smoothed by fewer bin widths.

Bensby et al. (2014) selected stars for spectroscopic study so that the sample contained extremes of both thin and thick disc. Therefore, many thin disc stars were necessarily neglected from the Bensby et al. (2014) sample. As a result, the sample contains a bias against high angular momentum stars. In Fig. 8, we compare the

Table 2. Estimated properties of the parent populations.

GIC	Age (Gyr)	N_1	N_2	$\langle L\rangle$ (km s^{-1} kpc)	σ_L	$\langle e\rangle$	σ_e
5	4.0	275 550	3786 181	1772	102	0.08	0.06
1	4.8	612 173	7573 869	1754	167	0.12	0.06
3	7.1	466 881	4993 675	1661	88	0.11	0.07
4	10.1	323 715	871 146	1511	266	0.25	0.11
2	10.2	315 132	1105 883	1601	310	0.23	0.11
6	12.1	80 620	267 500	1679	282	0.23	0.15

Notes. GIC is the group number given by Mitschang et al. (2014) and their estimated age given in Gyr. N_1 is the estimated size of the parent population computed using equation (1) and taking into account the probability of detecting an orbit in the solar neighbourhood. N_2 is the estimated size of the parent population computed using equation (4) and in addition corrects the probability with an estimate for the selection function for the observed sample. Mean eccentricity and angular momentum standard deviations are computed from the derived parent populations (shown in Fig. 10).

angular momentum distribution of the Bensby et al. (2014) sample to that of the GCS stars (Holmberg et al. 2009), but restricted to stars within 80 pc. In this figure, the blue histogram shows the Bensby et al. (2014) sample and the red histogram the GCS stars with overlaps displayed as purple.

We constructed a selection function, $f(L)$, choosing two tanh functions as they go smoothly between one constant to another constant value, and this allows us to model the two humps in the Bensby et al. (2014) sample evident in the angular momentum distribution shown in Fig. 8. The function we chose is described with a few parameters, is smooth, is never extremely small and does not cross zero (this is important as we need to divide by it). The black dots in Fig. 8 show the GCS histogram multiplied by $f(L)$ with

$$f(L) = a_0 - \frac{a_1}{2}\tanh\left(\frac{L-L_1}{s_1 L_{\rm LSR}}\right) - \frac{a_2}{2}\tanh\left(\frac{L-L_2}{s_2 L_{\rm LSR}}\right) \quad (2)$$

and coefficients $a_0 = 0.53, a_1 = 0.65, a_2 = 0.30, s_1 = 0.18, s_2 = 0.05$ and $L_1 = 1148, L_2 = 1445$ km s^{-1} kpc and with $L_{\rm LSR} = 1870$ km s^{-1} kpc. The function itself is plotted in Fig. 9. We did not automatically fit the coefficients, but did adjust the coefficients so that the two histograms lay on top of one another. Because we divide by this function, if it is an underestimate for the selection of the Bensby et al. (2014) sample, then we will overestimate the size of parent populations.

The function $f(L)$ is an estimate for the fraction of stars selected by Bensby et al. (2014) compared to that in the GCS. At L near that of the LSR, $f(L) \sim 0.05$ implying that for every high L star in the Bensby et al. (2014) sample, there are 20 stars with similar angular momentum in the GCS. At high angular momentum, the Bensby et al. (2014) sample also contains a higher proportion of high-eccentricity stars than the GCS. To ensure that we do not overestimate the number of high angular momentum high-eccentricity stars in the parent populations, we cut the selection function with

$$\begin{aligned} f(L,e) &= 1 \quad \text{for } L > 1600 \text{ km s}^{-1} \text{ kpc} \quad \text{and} \quad e > 0.15 \\ &= f(L) \quad \text{otherwise.} \end{aligned} \quad (3)$$

We correct the probability for each star in each abundance grouping with this selection function giving a total number for the parent population

$$N_2 = \sum_i \frac{1}{p_{\rm o}(e_i, L_i) f(L_i, e_i)} \quad (4)$$

again taking the minimum value for $p_{\rm o}$ within $e_i \pm \Delta e$ and $L_i \pm \Delta L$. The distribution of the parent populations for each abundance grouping, also taking into account the selection function, are shown in Fig. 10 and the numbers N_2 listed in Table 2. As expected the total number of stars estimated for each group is larger than that estimated previously without using the selection function. We integrate the parent distributions plotted in Fig. 10 in eccentricity to estimate angular momentum distributions. Likewise integrating in angular momentum, we can estimate eccentricity distributions. The estimated parent eccentricity distributions and the parent angular momentum distributions are shown as pink solid regions in Fig. 3 where numbers of stars in eccentricity bins of size 0.01 are plotted in the left-hand panels, and numbers of stars in angular momentum bins of size 20 km s^{-1} kpc are plotted in the right-hand panels.

4.1 Discussion on azimuthal structures and phase wrapping

To estimate the probability $p_{\rm o}$, we have assumed that the parent population is evenly distributed azimuthally in the galaxy. However, an originally cold disrupted cluster may not have time to become evenly distributed in azimuthal angle (for illustration see fig. 2 by Portegies Zwart 2009). This would lead to a bias – a survey of the solar neighbourhood would not see every group that is present at the Sun's galactocentric radius. Furthermore, the parent population size of a group detected in the solar neighbourhood would be overestimated by wrongly assuming that the group extended to all azimuthal angles.

Fig. 3 shows the eccentricity and angular momentum distributions of each group compared to the distributions estimated in the parent populations. This figure shows that the stars in a single group do not have the same angular momentum. The rotation period of a star in the galaxy can be estimated from a star's angular momentum. A spread in angular momentum in the group implies differential rotation between the higher and lower angular momentum members of the group. We consider how long it would take a disrupted cluster, with stars originally at the same azimuthal angle but with different angular momenta to shear out so that stars are located at every azimuthal angle in the Galaxy.

Because the angular rotation rate $\Omega \sim v_{\rm c}^2/L$ is approximately inversely proportional to the angular momentum, (with $v_{\rm c}$ the circular velocity and for an approximately flat rotation curve), the time it takes an initially compact cluster with a spread in angular momentum values dL to shear by 2π in azimuthal angle is

$$\Delta t \approx P\frac{L}{{\rm d}L} \quad (5)$$

with P the mean rotation period of the cluster. The rotation period at the solar neighbourhood is ∼0.24 Gyr. In 4 Gyr, there have been approximately 16 rotation periods giving d$L/L \sim 0.06$ for a group that has sheared by 2π and is now distributed at all azimuthal angles. Using a solar value of $L_{\rm LSR} = 1870$ for the cluster mean, we estimate d$L = 120$ km s^{-1} kpc is required for the cluster to shear to 2π at $\Delta t = 4$ Gyr. A parent population with a distribution with dispersion d$L \lesssim 120$ km s^{-1} kpc and age of 4 Gyr would not be evenly distributed in azimuthal angle. However, older populations with larger angular momentum dispersions would be evenly distributed in the Galaxy.

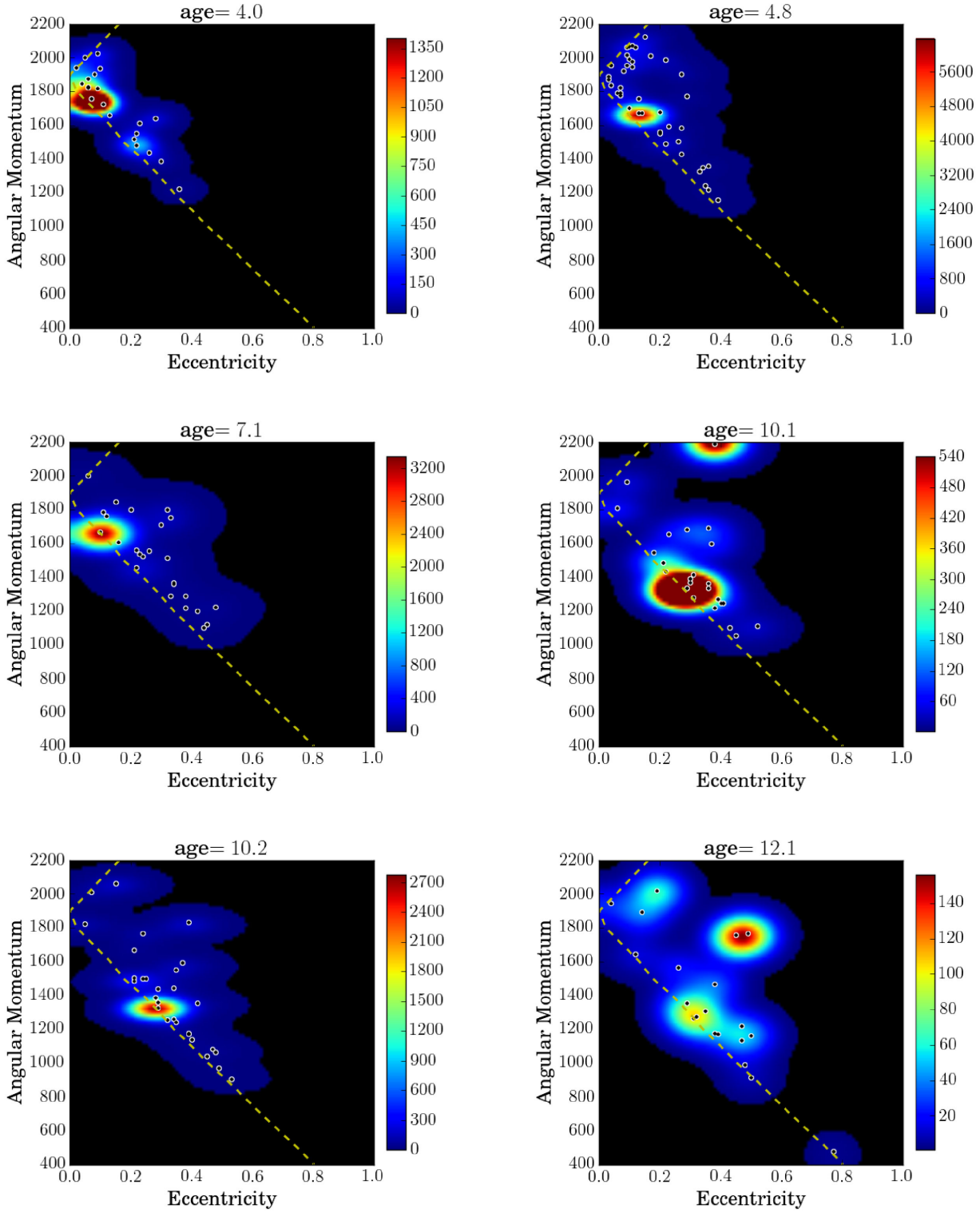

Figure 7. Distribution of parent populations of abundance groups, taking into account the orbital probability and using the eccentricities and angular momenta of the stars in the group. Each group can be identified by its age on the top of the plot. Eccentricity and angular momentum of stars in each abundance group are plotted as points on top of number density of the estimated parent distribution. Each panel shows a different abundance grouping with group properties listed in Table 1. The colour bar shows the estimated number of stars per eccentricity and angular momentum bin with bin width and height d$e = 0.01$ and d$L = 20$ km s^{-1} kpc. The dashed yellow lines border the forbidden region.

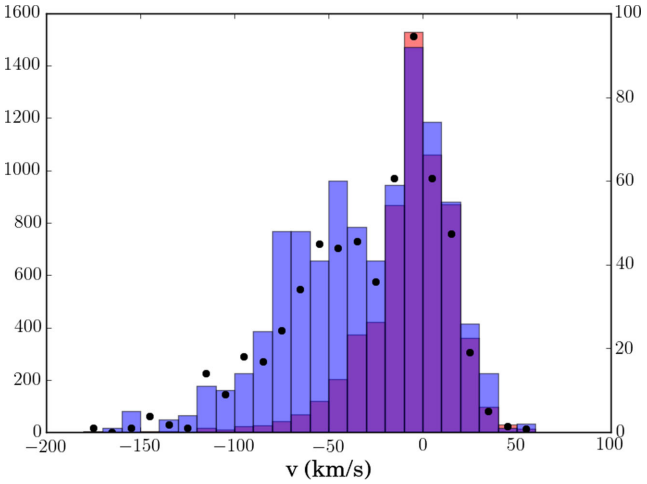

Figure 8. The angular momentum distribution of the Bensby et al. (2014) sample is shown in blue (with axis on the right) and that of the GCS in red (with axis on the left) with overlap regions shown in purple. The distributions are shown as a function of the V tangential velocity component and using 10 km s^{-1} kpc bins. The vertical axes show the number of stars in these bins. The GCS histogram when multiplied by the function in equation (2) is shown with black dots (with axis on the right). The black dots match the Bensby et al. (2014) histogram giving us an estimate of the selection bias compared to the GCS.

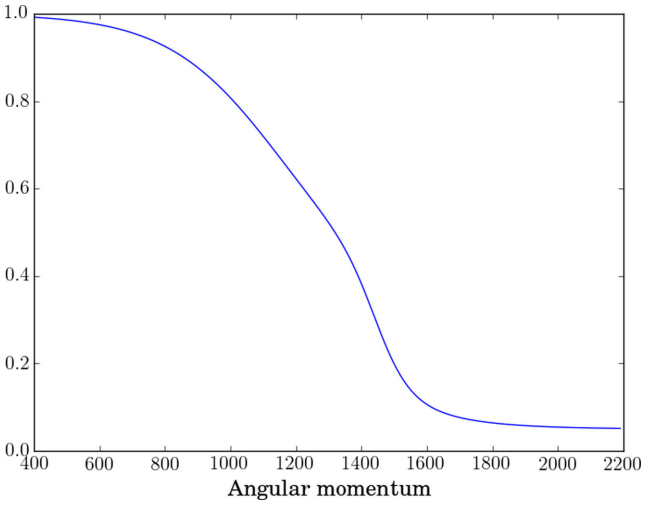

Figure 9. The selection function $f(L)$ (equation 2) is shown here as a function of angular momentum in km s^{-1} kpc. The Bensby et al. (2014) sample contains proportionally more low angular momentum stars than the GCS.

We use the rotation curve by Allen & Santillan (1991)[5] to compute the azimuthal angle

$$\theta(L) = \Omega(L)\Delta t \tag{6}$$

as a function of angular momentum for a population that is initially at the same azimuthal angle at birth. Here, Δt is the age of the group and θ is computed modulo 2π. After Δt, the more rapidly rotating stars (at lower angular momentum) will have increased in θ more than those rotating slower (at higher angular momentum). For three of the groups in Fig. 10, we show the angle $\theta(L)$ as a side panel. For the old groups, θ increases rapidly over a small change in angular momentum. As the angular momentum distributions for the old groups are large, they are likely to be well distributed in the Galaxy. In contrast, the younger groups contain peaks in the estimated parent populations that are narrow in angular momentum width, and θ varies relatively slowly across that width. In the peaks of the youngest two groups, we may have overestimated the parent populations by a factor of a few if they are not evenly distributed in the Galaxy. While we may have overestimated the number of stars in the youngest two groups (and for them only at angular momenta near that of the LSR), we have probably not overestimated the number of stars in the older groups.

In this discussion, we have neglected phase variations in the epicyclic angle. However, the epicyclic frequency is faster (about 40 per cent faster) than the angular rotation rate, so we expect the shearing in epicyclic angle takes place faster than in azimuthal angle.

Equation (6) assumes that stars were initially at the same azimuthal angle and had a similar angular momentum distribution. Heating and migration could have taken place well after the birth of the group. In this case, the group would be less evenly distributed than estimated using its age and its current angular momentum distribution. If the abundance group originated in a star cluster that remained bound for a long time before disrupting (e.g. Lamers & Gieles 2006), then the group would be less evenly distributed than estimated here. However, as a recently disrupted cluster should have a very narrow angular momentum distribution, more recent heating and migration rate would be required to account for wide current eccentricity and angular momentum distributions.

The parent populations appear to be clumpy, however, this could be due to sparse sampling. Alternately, phase wrapping due to shearing of azimuthal and epicyclic variations could also cause clumping along this boundary (Minchev et al. 2009). To estimate the parent population distributions, we divide by a probability that is sensitive to the eccentricity and angular momentum value near the forbidden boundary (as we can see from the sampling we used in Fig. 4). Along the forbidden region boundary, a small error in eccentricity or angular momentum could give a difference in probability of a factor of a few, and it is precisely in this region where most of the stars are located because that is the only region where the probability of finding a star is high. Errors in eccentricity and angular momentum measurements could cause the appearance of clumping near the forbidden boundary. We have minimized this effect by taking the maximum probability within the estimated errors for each data point. Nevertheless, a small variation in a star's eccentricity and angular momentum along this boundary causes a large change in probability, and we should be careful when interpreting structure in the parent populations.

We see from Figs 3, 7 and 10 that the youngest two groups have low-eccentricity means and dispersions. The estimated parent populations are large, greater than a million stars, the large size arising because a small fraction of the thin disc stars were selected for study by Bensby et al. (2014) and our correction for this selection increased the estimated number of parent stars. Both groups contain weak tails in the distribution extending to higher eccentricity. Only the 4.8 Gyr old grouping exhibits a tail towards higher angular momentum, corresponding to stars coming from outside the solar galactocentric radius. It is difficult to determine whether the parent population distribution has a large angular momentum dispersion (width) as the mean angular momentum values are near that of the Sun and low-eccentricity regions above and below this value lie in the forbidden region. If there was a large low-eccentricity

[5] The second term of equation (5) by Allen & Santillan (1991) should have the opposite sign.

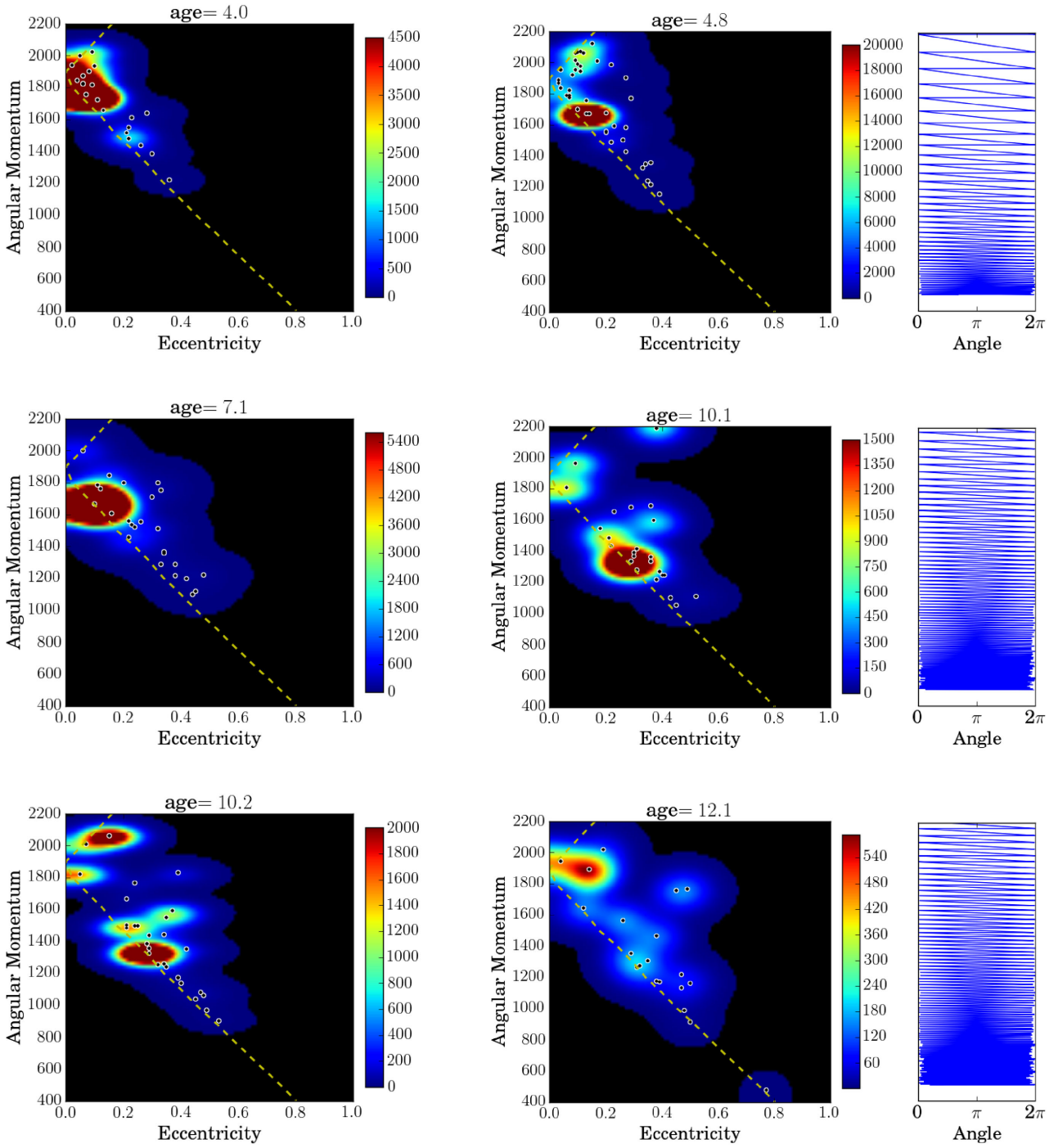

Figure 10. Distribution of parent populations of abundance groups. Similar to Fig. 7 except a bias against high angular momentum stars has been removed. Each panel shows a different abundance grouping with group properties listed in Table 1. Eccentricity and angular momentum of stars in each abundance group are plotted as points on top of number density of the estimated parent distribution. The dashed yellow lines border the forbidden region. On the right for three of the groups, we show an additional panel plotting the azimuthal angle $\theta(L)$ for a group originally at the same angle but after a time equal to the age of the group. The y-axis on these rightmost panels is angular momentum using the same scale as for the abundance distribution and the x-axis is the azimuthal angle θ. Only when $\theta(L)$ is slowly varying should we have overestimated the parent population by assuming an axisymmetric distribution. We have likely only overestimated the parent population size for the two youngest groups and only at angular momentum near 1800 km s^{-1} kpc.

population just interior to the Sun, then the higher eccentricity tails suggest that the eccentricity width of the parent population is wider at lower angular momentum than near $L \sim 1800$ km s^{-1} kpc. The estimated parent distributions suggest that most stars in the parent populations have not significantly migrated (changed in angular momentum) in the last 4–5 Gyr, though the tails in the parent distributions are significant. Perhaps, the same population that migrated also increased in eccentricity dispersion and a skewed Gaussian model for migration might be preferred (see fig. 3 by Bland-Hawthorn et al. 2010).

The 7.1 yr old group has a moderate width in its angular momentum distribution with a standard deviation of 200 km s^{-1} kpc and a mean of $L \sim 1640$ km s^{-1} kpc (and for comparison to the other groups see Table 2). The mean angular momentum value is below that of the LSR, and much of the parent population lies distant from the forbidden region, though the parent population could extend to lower angular momentum ($L \lesssim 1500$ km s^{-1} kpc) and low eccentricity ($e < 0.2$), and into the forbidden region. The tail of the distribution below $L = 1300$ km s^{-1} kpc and $e > 0.3$ suggests that the parent population could contain low-eccentricity stars below $L = 1300$ km s^{-1} kpc, as the eccentricity dispersion there is larger than at the mean $L \approx 1640$ km s^{-1} kpc. The parent angular momentum distribution (shown in Fig. 3) has one strong major peak, similar to those of the two youngest groups. In contrast, the three oldest groups have much wider angular momentum distributions (also see the standard deviations listed in Table 2). The shape of the parent population angular momentum distribution for the 7.1 old group suggests that many stars have not significantly migrated, however both width and fraction of stars in the low angular momentum tail are higher at 7.1 Gyr than for the two younger groups.

The peaks in the parent populations of the three youngest groups suggest that the bulk of their stars experienced little migration within 7 Gyr. Tails in the distributions imply that stars that have migrated in these groups have also increased in eccentricity dispersion. However, a thin disc group that increased in angular momentum dispersion (due to migration) without increasing in eccentricity dispersion would not have stars present in the solar neighbourhood unless its mean angular momentum was near that of the LSR.

As none of the peaks in the distributions (Fig. 10) for the three older groups contain many stars, we do not attribute any significance to the individual peaks. However, the oldest groups have both wide eccentricity and angular momentum parent distributions, suggesting that both heating and migration has taken place.

5 SUMMARY AND DISCUSSION

We summarize our primary findings here. A discussion follows.

(1) We find that stars in the six largest abundance groups by Mitschang et al. (2014) tend to lie near a boundary in angular momentum versus eccentricity space where the probability is highest for a star to be found in the solar neighbourhood, assuming a relaxed parent population evenly distributed in azimuthal and epicyclic angles. The stars that are most likely found are those with orbital apocentre approximately equal to the Sun's galactocentric radius. The bias has previously been described as a crossing time bias (Mayor et al. 1977).

(2) Using the probability for a star to be located in the solar neighbourhood (as a function of eccentricity and angular momentum) and a crudely estimated selection function for the sample, we estimate that the parent populations of the abundance groups range from 200 000 to a few million members.

(3) The two youngest groups lie nearest forbidden boundaries, implying that there could be a significant population of group stars that cannot be seen in the solar neighbourhood. However, the two youngest groups are the least likely to be evenly distributed azimuthally in the Galaxy and by assuming an even distribution, we may have over estimated the size of the parent populations by a factor of a few. The angular momentum dispersions of the older groups imply that the parent populations are distributed at all azimuthal angles in the Galaxy and that we have not overestimated the sizes of their parent populations.

(4) Assuming that mean angular momentum is similar to that at birth, the width of the parent populations of the thin disc groups suggest that the bulk of their stars experienced little migration within 7 Gyr. Tails in the distributions suggest that stars that have migrated in these groups have also increased in eccentricity dispersion. In contrast, the parent populations of the thick disc groups exhibit both wide angular momentum and eccentricity distributions suggesting that both heating and radial migration has taken place.

Here, we assumed that eccentricity and inclination distributions are not correlated and have ignored the vertical motions. Using the vertical velocities, it is possible to estimate the inclination distribution of the parent populations. Stars with high inclination are less likely to be detected within 100 pc of the Sun (Mayor et al. 1977), and we have not taken this into account in our estimate of the parent populations. The numbers of stars in the older groups, with the highest vertical amplitudes, have been underestimated by a factor of a few due to this neglect.

A large cluster may self-pollute with supernova and so may not remain chemically homogeneous. Consequently, single abundance populations are estimated to have sizes below 2×10^5 stars (section 3.2 by Bland-Hawthorn et al. 2010). The large sizes for the parent populations estimated here are a concern as they are above this limit. One possibility is that each group may be comprised of similar but not identical fragments (Mitschang et al. 2014). Or the large groups may be part of a coeval population composed of stars born nearly at the same *time*, and with similar abundances (Blanco-Cuaresma et al. 2015), but not necessarily all born in the same *place* (a coeval but not necessarily conatal parent population). Alternatively, the large parent population sizes could be attributed to overestimation resulting from our assumption of an axisymmetric and mixed parent distribution. Smaller abundance groups were found by Mitschang et al. (2014), and these would be consistent with the smaller parent sizes estimated for chemically homogenous populations.

We mention some uncertainties that affect this study. Bensby et al. (2014) gave no selection description for their entire sample. We crudely modelled the Bensby et al. (2014) sample distribution by comparing it with the GCS, however, the GCS sample itself is taken from two different magnitude-limited source catalogues and is only complete to 40 pc (Nordström et al. 2004). Future attempts to study parent populations of abundance groups will be more robust if they are based on well-characterized samples, and well-characterized samples would allow more robust estimates of parent populations.

In this study, we used a Monte Carlo simulation technique to estimate the probability that an orbit family would be detected in the solar neighbourhood. We then used this probability distribution and the stars in each group to estimate the parent population distributions. However, different distributions for the parent populations could be assumed from the start and Monte Carlo simulations used to predict the number and distribution of stars detected in the solar neighbourhood. This approach might alleviate some of the difficulties caused by the sparse sampling resulting from the few stars in each group.

As did Bensby et al. (2014), we adopted the Milky Way model by Allen & Santillan (1991). This study could be redone with different or updated Milky Way mass distributions to see how the estimated parent populations are dependent upon the underlying assumed Galactic mass distribution. Both accurate space motions and a good Milky Way mass model are needed to better estimate the parent population distributions, particularly for stars near the forbidden boundary where the probability is a strong function of eccentricity and angular momentum.

We assumed a sharp edged spherical boundary at 100 pc from the Sun for the solar neighbourhood sample. However, approximately 5 per cent of the stars from the six abundance groups are at larger distances. Future work could study the impact of a selection function that depends on distance from the Sun. Errors in measurement of eccentricities and angular momenta have been neglected from this study. These too could be more accurately modelled.

Azimuthal structure in the probability distributions has been ignored in this study; however, the probability distributions could be sensitive to position with respect to the Galactic bar, spiral arms and other dynamical structures such as the Galactic warp.

Future studies may detect variations in the orbital properties of the groups in different directions allowing a study of azimuthal variations and correlations between orbital properties as a function of distance from the Sun. As more stars are identified in a single group, it will be possible to determine whether clumps in e, L are real. Clumps along the region of high probability in e, L space might arise because of a non-uniform distribution in epicyclic amplitude (e.g. see Minchev et al. 2009). The location of peaks in the distribution might depend on distance from the Sun, particularly if the group is not well mixed in the Galaxy. Detected structures would be exciting to study with models of how groups evolve as they move in the Galaxy.

In summary, we were surprised by the large sizes of our estimated parent populations. The large sizes imply that large abundance groups found in the vicinity of the Sun are unlikely to be conatal populations unless they are unevenly distributed in the Galaxy. If the groups are not conatal, then they may not be comprised of stars exactly the same age. The colour–magnitude diagram fits to the abundance groups were no worse than those of open clusters (Mitschang et al. 2014), suggesting that if there is an age spread in each group, it is not large. However, an age spread in the stars in the low metallicity groups might contribute to the large eccentricity and angular momentum dispersions of these groups. Likewise, the higher metallicity groups may have lower angular momentum and eccentricity dispersions simply because they are comprised of younger and thin disc stars. Despite these concerns, the increasingly large samples of stars with accurate abundance measurements (e.g. De Silva et al. 2015) should be used to study groups of stars with similar abundances and may be used to probe mechanisms such as migration. However, constraints on the dynamical evolution of stellar subpopulations will require larger and better characterized samples, samples that extend away from the solar neighbourhood and comparisons between observed and predicted distributions of many streams and groups.

ACKNOWLEDGEMENTS

We thank Segev Benzvi, Cameron Bell, Chelsea Jean, Eva Bodman and Eric Mamajek for helpful discussions and correspondence. BA and DBZ gratefully acknowledge the financial support of the Australian Research Council through Super Science Fellowship FS110200035 and Future Fellowship FT110100743, respectively. This work was in part supported by NASA grant NNX13AI27G. The authors would like to thank members of the Macquarie University and Australian Astronomical Observatory joint Galactic archaeology group for helpful discussions.

REFERENCES

Adibekyan V. Zh. et al., 2013, A&A, 554, 44
Allen C., Santillan A., 1991, Rev. Mex. Astron. Astrofis., 22, 255
Anders F. et al., 2014, A&A, 564, 115
Bedin L. R., Piotto G., Carraro G., King I. R., Anderson J., 2006, A&A, 460, L27
Bensby T., Feltzing S., Oey M. S., 2014, A&A, 562, 71
Blanco-Cuaresma S. et al., 2015, A&A, submitted
Bland-Hawthorn J., Krumholz M. R., Freeman K., 2010, ApJ, 713, 166
De Silva G. M., Sneden C., Paulson D. B., Asplund M., Bland-Hawthorn J., Bessell M. S., Freeman K. C., 2006, AJ, 131, 455
De Silva G. M., Freeman K. C., Bland-Hawthorn J., Asplund M., Bessell M. S., 2007, AJ, 133, 694
De Silva G. M. et al., 2015, MNRAS, 449, 2604
Freeman K., Bland-Hawthorn J., 2002, ARA&A, 40, 487
Fuhrmann K., 2011, MNRAS, 414, 2893
Haywood M., Di Matteo P., Lehnert M. D., Katz D., Gomez A., 2013, A&A, 560, 109
Holmberg J., Nordström B., Anderson J., 2009, A&A, 501, 941
Kruijssen J. M. D., Pelupessy F. I., Lamers H. J. G. L. M., Portegies Zwart S. F., Icke V., 2011, MNRAS, 414, 1339
Lamers H. J. G. L. M., Gieles M., 2006, A&A, 455, L17
Lehnert M. D., Di Matteo P., Haywood M., Snaith O. N., 2014, ApJ, 789, L30
Liu C., Ruchti G., Feltzing S., Martínez-Barbosa C. A., Bensby T., Brown A. G. A., Portegies Zwart S. F., 2015, A&A, 575, A51
Mayor M., Martinet L., Turon Lacarrieu C., 1977, A&A, 61, 433
Minchev I., Quillen A. C., Williams M., Freeman K. C., Nordhaus J., Siebert A., Bienaymé O., 2009, MNRAS, 396, 56
Minchev I., Chiappini C., Martig M., 2013, A&A, 558, 9
Minchev I. et al., 2014, ApJ, 781, L20
Mitschang A. W., De Silva G., Zucker D. B., Anguiano B., Bensby T., Feltzing S., 2014, MNRAS, 438, 2753
Navarro J. F., Abadi M. G., Venn K. A., Freeman K. C., Anguiano B., 2011, MNRAS, 412, 1203
Nordström B. et al., 2004, A&A, 418, 989
Portegies Zwart S. F., 2009, ApJ, 696, L13
Quillen A. C., 2002, AJ, 124, 400
Quillen A. C., 2014, Feltzing S., Zhao G., Walton N.A., Whitelock P. A., eds, Proc. IAU Symp. 298, Setting the Scene for Gaia and LAMOST. Cambridge Univ. Press, Cambridge, p. 105
Quillen A. C., Minchev I., Bland-Hawthorn J., Haywood M., 2009, MNRAS, 397, 1599
Quillen A. C., Dougherty J., Bagley M. B., Minchev I., Comparetta J., 2011, MNRAS, 417, 762
Reddy B. E., Lambert D. L., Allende Prieto C., 2006, MNRAS, 367, 1329
Schönrich R., Binney J., 2009, MNRAS, 396, 203
Schönrich R., Binney J., Dehnen W., 2010, MNRAS, 403, 1829
van Leeuwen F., 2007, A&A, 474, 653

This paper has been typeset from a TEX/LATEX file prepared by the author.